processes

MDPI

Article

Simultaneous Adsorption of 4,6-Dimethyldibenzothiophene and Quinoline over Nickel and Boron Modified Gamma-Al_2O_3 Adsorbent

Esteban Camu [1,*], Barbara Pasten [1], Camila Matus [1], Fernanda Ramirez [1], Juan Ojeda [2], Gonzalo Aguila [3] and Patricio Baeza [1,*]

1 Instituto de Química, Pontificia Universidad Católica de Valparaíso, Casilla 4059, Valparaíso, Chile; barbara.pasten.lira@gmail.com (B.P.); camila.matus@gmail.com (C.M.); fernandaramirez1@gmail.com (F.R.)
2 Escuela de Nutrición, Facultad de Farmacia, Universidad de Valparaíso, Casilla 4059, Valparaíso, Chile; juan.ojeda@uv.cl
3 Departamento de Ciencias de la Ingeniería, Facultad de Ingeniería, Universidad Andres Bello, Antonio Varas 880, Santiago, Chile; gonzalo.aguila@unab.cl
* Correspondence: patricio.baeza@pucv.cl (P.B.); esteban.camu.m@mail.pucv.cl (E.C.)

Received: 27 February 2020; Accepted: 27 March 2020; Published: 2 April 2020

Abstract: The simultaneous adsorption of quinoline and 4,6-dimethyldibenzothiophene over adsorbents, based on alumina modified with boron and nickel under ambient temperature and pressure, was studied. The adsorbents were characterized by BET specific surface area, a potentiometric method for the determination of acid strength, electrophoretic migration, and X-ray diffraction. The results showed that the adsorbent containing nickel had better adsorption capacity than the adsorbent modified with nickel and boron, which was attributed to its greater acidity and ability to generate π-complexation between the adsorbent and the molecules. In terms of selectivity, quinoline was more adsorbed than 4,6-dimethyldibenzothiophene in all systems, due to the basic nature of quinoline. The experimental data in all cases were adjusted by three kinetic models (Yoon–Nelson, Yan and Thomas), and the regression coefficients in all models were close to one. Finally, the values of the kinetic constant obtained by the Thomas model were used to relate the adsorption capacity results.

Keywords: adsorption; 4,6-dimethyldibenzothiophene; quinoline; alumina; boron; nickel

1. Introduction

Diesel is a complex mixture of hydrocarbons formed by organosulfur and organonitrogen molecules, among other compounds. The combustion of these molecules is responsible for environmental pollution, acid rain and health problems. Also, the sulfur compounds can poison the catalysts used in catalytic converters [1], while the nitrogen compounds inhibit the removal of sulfur compounds [2]. To eliminate these pollutants, different hydrotreating (HT) reactions, specifically hydrodesulfurization (HDS) and hydrodenitrogenation (HDN), are carried out during the refining of petroleum. These processes use Co-Mo/γ-Al_2O_3, Ni-Mo/γ-Al_2O_3 or Ni-W/γ-Al_2O_3 catalysts at high temperatures (300–400 °C) and under elevated hydrogen pressures (20–100 atm).

However, due to depletion of continental crude oil deposits, the deeper reservoirs of petroleum contain a large number of sulfur and nitrogen polynuclear aromatic molecules that are refractory to the conventional methodologies. To eliminate these compounds, new costly processes of HT that produce considerable amounts of carbon must be applied. In order to economize the desulfurization or denitrogenation processes, other milder methods must be developed. In this regard, several research groups have studied the elimination of these types of molecules by adsorption [3–7], which, unlike HT reactions, is carried out at ambient temperature and pressure. Despite there being a wide variety

of solids used as adsorbents, alumina is one of the main supports used in HT reactions [8–13] and has shown the capacity to remove sulfur and nitrogen compounds simultaneously by adsorption, as described by Kim et al. [4].

Over the years, it has been studied how to improve the activity of HT catalysts, by incorporating different additives [14–21]. Similarly, in the case of adsorbent systems, different additives have been studied to improve adsorption capacity [6,22,23]. On this matter, the incorporation of nickel in different porous materials has been widely studied [7,24,25], due to the high adsorption capacity of this metal on diverse pollutants. However, in our previous work [3], we have shown that the incorporation of 4% nickel on alumina decreases the adsorption capacity of pyridine, due to the formation of $NiAl_2O_4$. On the other hand, the incorporation of boron has shown an improvement in the activity of HT catalysts, which is mainly associated with the modification of the acidity and dispersion of the active metals [26,27]. However, at higher boron loadings of over 1.8 wt%, poor catalytic performance was observed due to the presence of a bulk borate phase [28]. Moreover, better dispersions of active phases were achieved at boron loadings of 0.6 wt% [29], while that of other studies have shown that the addition of 0.5 wt% B to a NiMo catalyst caused a decrease in the intensity of the alumina diffraction line, due to the formation of a microcrystalline aluminum borate phase on the catalyst surface [30]. The incorporation of boron for the adsorption of sulfur compounds has also been studied. Recently, Zheng et al. [22] incorporated B_2O_3 at Ag-CeOx/TiO_2-SiO_2 adsorbent, obtained a high dispersion of CeOx, and as a consequence, higher adsorptive desulfurization activity.

In this context, this work evaluated the influence of boron on the acidity and dispersion values of the Ni/Al_2O_3 adsorbent system used in the simultaneous adsorption of 4,6-dimethyl-dibenzothiophene (4,6-DMDBT) and quinoline (QN), as model compounds for sulfur and nitrogen, respectively. Additionally, the experimental adsorption curves in all cases were fitted by three kinetic models: Yoon-Nelson [31], Yan [32], and Thomas [33], that are commonly used in fixed bed adsorption studies in order to analyze the column performance.

2. Materials and Methods

2.1. Preparation of the Adsorbents

Gamma alumina (BASF D10-10) was modified with 0.4 wt% of boron (B(0.4) γ-Al_2O_3) and with 4.0 wt% of nickel (Ni(4.0) γ-Al_2O_3), using the wet impregnation method. The incorporation of boron was realized with H_3BO_3 (Sigma Aldrich p.a.) using the required amount to obtain a 0.4 wt% of boron. Then, the adsorbent was dried at 378 K overnight and then calcined in air at 823 K for 4.5 h. The Ni-modified alumina adsorbent was obtained with the required amount of $Ni(NO_3)_2{\cdot}6H_2O$ to obtain a 4.0 wt% of nickel. This adsorbent was dried at 378 K overnight and calcined in air at 823 K for 4.5 h. The Ni and boron modified alumina adsorbent (Ni(4.0)B(0.4) γ-Al_2O_3) was obtained by wet impregnation of $Ni(NO_3)_2{\cdot}6H_2O$ over B(0.4) γ-Al_2O_3, then were dried at 378 K overnight and calcined in air at 823 K for 4.5 h.

2.2. Characterizations of the Adsorbents

The determination of the specific surface area (S_{BET}) [34] for each adsorbent was done in a Micromeritics ASAP-2010 apparatus for volumetric nitrogen adsorption-desorption, using 0.2–0.4 g of each sample, which were degassed at 120 °C for 18 h, reaching a final pressure of 1×10^{-3} mmHg. Subsequently, the analysis was performed within a glass slide at 77 K. The determination of the Isoelectric Point (IEP) was realized by electrophoretic migration, as in previous studies [15]. The surface acidity of the adsorbents was measured by potentiometric titration [35]. The X-ray diffraction patterns of the powder samples were made in a Panalytical X'Pert diffractometer equipped with an Xcelerator detector with automatic divergence slits and Cu $K_{\alpha1/\alpha2}$ radiation (40 kV, 40 mA). The K-beta radiation of Cu was excluded using nickel filters and the K-alpha2 radiation was removed arithmetically using the Panalytical HighScore Plus Software. The positions of the peaks and the profiles were adjusted by

the Pseudo-Voigt function and the WinXPow software. The identification of the phases was carried out using the PDF-2 database of the International Center of Diffraction Data (ICDD).

2.3. Adsorption Experiments

Adsorption experiments were performed at ambient temperature and pressure using a vertical Pyrex reactor equipped with a supporting glass porous disk. A bed of 500 mg of adsorbent was placed in the reactor. Prior to the determination of the adsorption capacity (q_e), a surface cleaning process was performed for each adsorbent, with a 20 mL min^{-1} flow of pure Ar at 378 K for 1 h and subsequent cooling to room temperature. For the adsorption experiments, the liquid flow was driven into the reactor by means of a variable flow peristaltic mini-pump. The experiment was performed using a mixture of 250 ppmw of QN and 250 ppmw 4,6-DMDBT in isooctane at a feed rate (Q) of 0.5 mL min^{-1}. Samples were collected every 10 min, until saturation of the adsorbent was reached; the total time and number of samples depended on the adsorption capacity of the adsorbent.

The samples were analyzed by gas chromatography with a flame ionization detector (GC-FID), using a Shimadzu GC-2010 equipped with an SPB-5 capillary column (L 30 m, I.D. 0.25 mm, Film 0.25 mm), and the following conditions: detector at 553 K, injector at 523 K, and carrier flow, 30 mL min^{-1} (N_2). The column temperature was set to increase from 433 K to 513 K at a rate of 20 K min^{-1}; 1.0 μL of the sample volume was injected, using an autosampler, for each GC-FID run.

The adsorption results for the different systems studied were represented as adsorption curves (adsorbed fraction vs eluted volume), where the adsorbed fraction is expressed as 1-(C_t $C_0{}^{-1}$), where C_t corresponds to the concentration of QN at time t (after adsorption) and C_0 is the feed concentration.

The QN and 4,6-DMDBT adsorbed per unit mass of the adsorbent (q_e), and was calculated using Equation (1). The selectivity was studied with the relative selectivity factor used by Kim et al. [4] (Equation (2)), where q_{ei} and q_{en} are the adsorption capacity for QN and 4,6-DMDBT, respectively.

$$q_e = C_0 \int_{t=0}^{t} \left(1 - C_t \times C_0^{-1}\right) dt \quad (1)$$

$$\alpha_{i-n} = \frac{q_{ei}}{q_{en}} \quad (2)$$

2.4. Adsorption Kinetics

To estimate the kinetic parameters that govern the adsorption process in a fixed bed system, several mathematical models have been studied by different research groups, and many of them are summarized in a review by Xu et al. [36]. Each of these models describes the dynamic behavior of the adsorption curves and attempts to relate experimental data with those calculated by the prediction model. For the estimation of the parameters of each model, the non-linear analysis of the curves (C_t $C_0{}^{-1}$ vs. t) was performed, using the nonlinear curve fit available in Origin 8.0 Software.

2.5. Kinetics Models

2.5.1. Yoon–Nelson Model

The Yoon–Nelson model is extremely concise in its form for the prediction of mass transfer phenomena. This model assumes the adsorption rate is proportional to the adsorption capacity of the solid and the initial concentration of feed. The nonlinear form of this model is presented in Equation (3).

$$\frac{C_t}{C_0} = \frac{1}{1 + e^{k_{YN}(\tau - t)}} \quad (3)$$

where k_{YN} correspond to the Yoon–Nelson velocity constant (min^{-1}), and τ (min) denotes the adsorption time when 50% has been reached in adsorbate extraction.

2.5.2. Yan Model

This model is a variation of the Dose–Response model, initially developed for pharmacological studies. This model has recently been used to describe the kinetics of metal adsorption [32], however it is interesting to study its behavior in the study of adsorption of organic molecules. This model is represented by Equation (4).

$$\frac{C_t}{C_0} = 1 - \frac{1}{1 + \left(\frac{C_0\ Q\ t}{q_e m}\right)^a} \quad (4)$$

where q_e is the maximum concentration of the adsorbate on the surface of the adsorbent (mg g^{-1}), and a corresponds to the dimensionless constant of the model.

2.5.3. Thomas Model

This model is used to estimate the adsorption capacity (q_e) of an adsorbent and predict adsorption curves, assuming second order reversible kinetics. This model is based on the Langmuir isotherms, so the adsorption process is not limited only by the reaction on the surface, but also by the phenomena of mass transfer in the liquid–solid interface. This model is described by Equation (5).

$$\frac{C_t}{C_0} = \frac{1}{1 + e^{[(k_{th}\ q_e\ m/Q) - (k_{th}\ C_0\ t)]}} \quad (5)$$

where C_t corresponds to the concentration of the adsorbate at time t, k_{th} corresponds the Thomas velocity constant (mL min^{-1} mg^{-1}), Q is the feed flow (mL min^{-1}), q_e is the maximum concentration of the adsorbate on the surface of the adsorbent (mg g^{-1}), m is the mass of adsorbent (g), and C_0 corresponds to the initial concentration of the adsorbate (mg mL^{-1}).

3. Results and Discussion

The results of characterization by BET method, acid strength and isoelectric point of adsorbents are shown in Table 1.

Table 1. Characterization results for γ-Al_2O_3 modified with boron and nickel.

Adsorbent	Specific Surface Area (m^2 g^{-1})	Pore Diameter (nm)	Acid Strength (mV)	Isoelectric Point (pH)
γ-Al_2O_3	213	6.8	−61.7	8.02
B(0.4) γ-Al_2O_3	170	8.2	−33.1	7.93
Ni(4.0) γ-Al_2O_3	209	6.9	−6.8	6.80
Ni(4.0) B(0.4) γ-Al_2O_3	197	10.8	−27.5	7.25

Initially, it can be observed that the specific surface area of γ-alumina decreases from 213 to 170 and 209 m^2 g^{-1} for B(0.4) γ-Al_2O_3 and Ni(4.0) γ-Al_2O_3, respectively, when boron and nickel are incorporated into this support. For the nickel modified adsorbent, the slight decreases in the specific surface area could be related to the pore obstruction of support by the presence of the metal. For the boron modified adsorbent, despite the decrease in the specific surface area values, an increase in the pore diameter values was observed. This behavior can be due to the formation of new pores in the γ-Al_2O_3 by the incorporation of boron or for the obstruction of pores with minor diameter, which was also observed by Engelso et al. [37] when studying the boron incorporation on alumina. These authors suggest that with boron incorporation, the diameters of pores < 10 nm will be diminished, and new pores > 50 nm will appear.

On the other hand, the acid strength values listed in the Table 1, shows an increase in the values of B(0.4) γ-Al_2O_3 (−33.1) and Ni(4.0) γ-Al_2O_3 (−6.8) adsorbents with respect to pure alumina (−61.7). This behavior can be related with the formation of new Lewis and Brönsted sites by the incorporation

of nickel to the alumina [25,26], and the formation of new Brönsted sites caused by the incorporation of boron.

For the case of electrophoretic migration measures, a decrease in the values of IEP of alumina (8.02) to 7.93 and 6.80 is observed, when boron and nickel were incorporated to this support, respectively (see Table 1). In the case of nickel, this decrease can be due to the formation of nickel aluminate type ($NiAl_2O_4$) species with lower values of IEP near to 2.7 [38]. For boron incorporation, the decrease in the IEP value can be explained by the formation of negative surface complexes with boric acid [39]. For the Ni(4.0)-B(0.4) γ-Al_2O_3 adsorbent, intermediate values of acid strength and IEP are obtained with respect to the incorporation of elements separately. This result is somehow expected, taking into account that the possible location of Ni species on the boron-alumina surface.

The XRD diffractograms of the different adsorbents are shown in Figure 1.

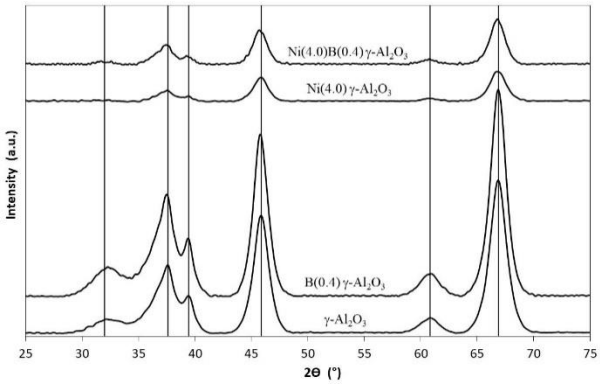

Figure 1. XRD diffractograms obtained for the different adsorbents. The characteristics diffraction lines of γ-Al_2O_3 (———) are indicated as reference.

In the case of alumina, the characteristic diffraction peaks of γ-Al_2O_3 (included in Figure 1 as reference) can be clearly seen. When boron is incorporated into alumina, the diffractogram of the B(0.4) γ-Al_2O_3 adsorbent does not show significant variation with respect to pure γ-Al_2O_3, presenting the same diffraction peaks, and no crystalline boron oxide species (B_2O_3) were detected. Therefore, in the case of the B(0.4) γ-Al_2O_3 adsorbent, it could be noted that there are no crystalline or agglomerated B species, and it is proposed that B species are highly dispersed on the surface of γ-Al_2O_3, possibly forming a thin coating or monolayer, which cannot be detected by XRD. The above can be based on the low loading of B (0.4 wt %) with respect to the high specific surface area of the alumina (see Table 1). In addition, in the diffractogram of the B(0.4) γ-Al_2O_3 adsorbent, it is possible to observe a slight increase in the intensity of the diffraction peaks, that is, a slight increase in the crystallinity of γ-Al_2O_3. One reason for this increase in the crystallinity of γ-Al_2O_3 could be related to the calcination temperature of the B(0.4) γ-Al_2O_3 adsorbent (823 K for 4.5 h).

In the case of the Ni(4.0) γ-Al_2O_3 adsorbent, it can be seen in Figure 1 that its diffractogram is similar to that obtained in pure γ-Al_2O_3, but unlike that with B(0.4) γ-Al_2O_3 adsorbent, in this adsorbent the incorporation of nickel on the alumina produces a notable decrease in intensity of the diffraction peaks corresponding to γ-Al_2O_3, as seen in Figure 1, which represents a loss of crystallinity in Ni(4.0) γ-Al_2O_3 adsorbent. The above behavior could be explained considering the higher Ni load than B load (4.0 > 0.4 wt%) on the alumina support. However, this 4.0 wt% of Ni loading is not so high as to exceed the dispersion capacity of alumina support, remembering that its specific surface area is 213 $m^2\ g^{-1}$ (see Table 1). In fact, the Ni(4.0) γ-Al_2O_3 adsorbent has a specific surface area of 209 $m^2\ g^{-1}$, almost the same as the specific surface area of γ-Al_2O_3. Therefore, Ni loading (4.0 wt%) does not affects alumina specific surface area but does affect its crystallinity as mentioned above. In addition, in the diffractogram of the Ni(4.0) γ-Al_2O_3 adsorbent, it is not possible to observe nickel oxides species (NiO, Ni_2O_3), so it is likely that Ni species formed on the alumina are highly dispersed, cannot be detected by XRD, or Ni species are in an agglomerate with low crystallinity or amorphous state, but this last

explanation is less probable. Finally, in the case of the diffractogram of the Ni(4.0) B(0.4) γ-Al_2O_3 adsorbent, it presents a similar result to the Ni(4.0) γ-Al_2O_3 adsorbent (see Figure 1), i.e., a decrease in the intensity of the diffraction peaks corresponding to γ-Al_2O_3. The XRD analysis of the Ni(4.0) B(0.4) γ-Al_2O_3 adsorbent could be summarized as a weighted combination of the B(0.4) γ-Al_2O_3 and Ni(4.0) γ-Al_2O_3 adsorbents, considering that the Ni(4.0) B(0.4) γ-Al_2O_3 adsorbent presents different metals loads on alumina (Ni loading is 10 times more than B loading), and as it was noted above, the incorporation of B on γ-Al_2O_3 produces an increase in the crystallinity of alumina, the subsequent incorporation of Ni on B(0.4) γ-Al_2O_3 produces a loss in its crystallinity.

In addition, in the diffractogram of the Ni(4.0) B(0.4) γ-Al_2O_3 adsorbent, it is not possible to identify the presence of boron and nickel oxides, which would indicate that the presence of B at the concentration used, does not affect the dispersion of Ni. It is worth recalling the BET area results of these adsorbents (see Table 1), where it is shown that the incorporation of B on alumina produce a decrease in its specific surface area, from 213 to 170 $m^2\ g^{-1}$, unlike the incorporation of Ni that does not produce changes in the specific surface area of γ-Al_2O_3, from 213 to 209 $m^2\ g^{-1}$. It is interesting to note that when Ni is incorporated on boron-modified alumina, which corresponds to Ni(4.0) B(0.4) γ-Al_2O_3 adsorbent, there is an increase in its specific surface area, from 170 to 197 $m^2\ g^{-1}$ (see Table 1).

This last result with the XRD results (see Figure 1), allows us to propose that Ni species would be interacting with surface B species, forming highly dispersed Ni-B species, since they are not detected by XRD, but at the same time this Ni-B species could be responsible of increasing the specific surface area of the Ni(4.0) B(0.4) γ-Al_2O_3 adsorbent with respect to the B(0.4) γ-Al_2O_3 adsorbent. The possible existence of Ni-B species interacting on the surface of the alumina will be discussed later.

3.1. Adsorption Tests

The breakthrough curves, obtained for the adsorption of mixed 4,6-DMDBT and QN on the different adsorbents, are shown in Figure 2. The experimental adsorption capacity (q_e) and selectivity ($\alpha_{i\text{-}n}$), determined by Equations (1) and (2), respectively for 4,6-DMDBT and QN are summarized in Table 2. The results of this table show that all systems studied adsorbed higher amounts of QN than 4,6-DMDBT. This behavior can be attributed to the strong interaction between the Al(III) sites on γ-Al_2O_3 with the electronic pair of the nitrogen atom of QN that acts as a Lewis base [40]. In the case of 4,6-DMDBT, the steric hindrance effect of the methyl groups of this molecule generate a decrease in the interaction between OH functional groups of γ-Al_2O_3 with the aromatic rings of 4,6-DMDBT, producing lower adsorption.

Table 2. Experimental adsorption capacity and selectivity for 4,6-DMDBT and QN.

Adsorbent	$q_{e(4,6\text{-DMDBT})}$ (mg g^{-1})	$\alpha_{i\text{-}n\ (4,6\text{-DMDBT})}$	$q_{e(QN)}$ (mg g^{-1})	$\alpha_{i\text{-}n\ (QN)}$
γ-Al_2O_3	7.02	1.00	22.29	3.17
B(0.4) γ-Al_2O_3	8.72	1.00	23.69	2.72
Ni(4.0) γ-Al_2O_3	9.77	1.00	32.67	3.34
Ni(4.0) B(0.4) γ-Al_2O_3	6.51	1.00	21.02	3.23

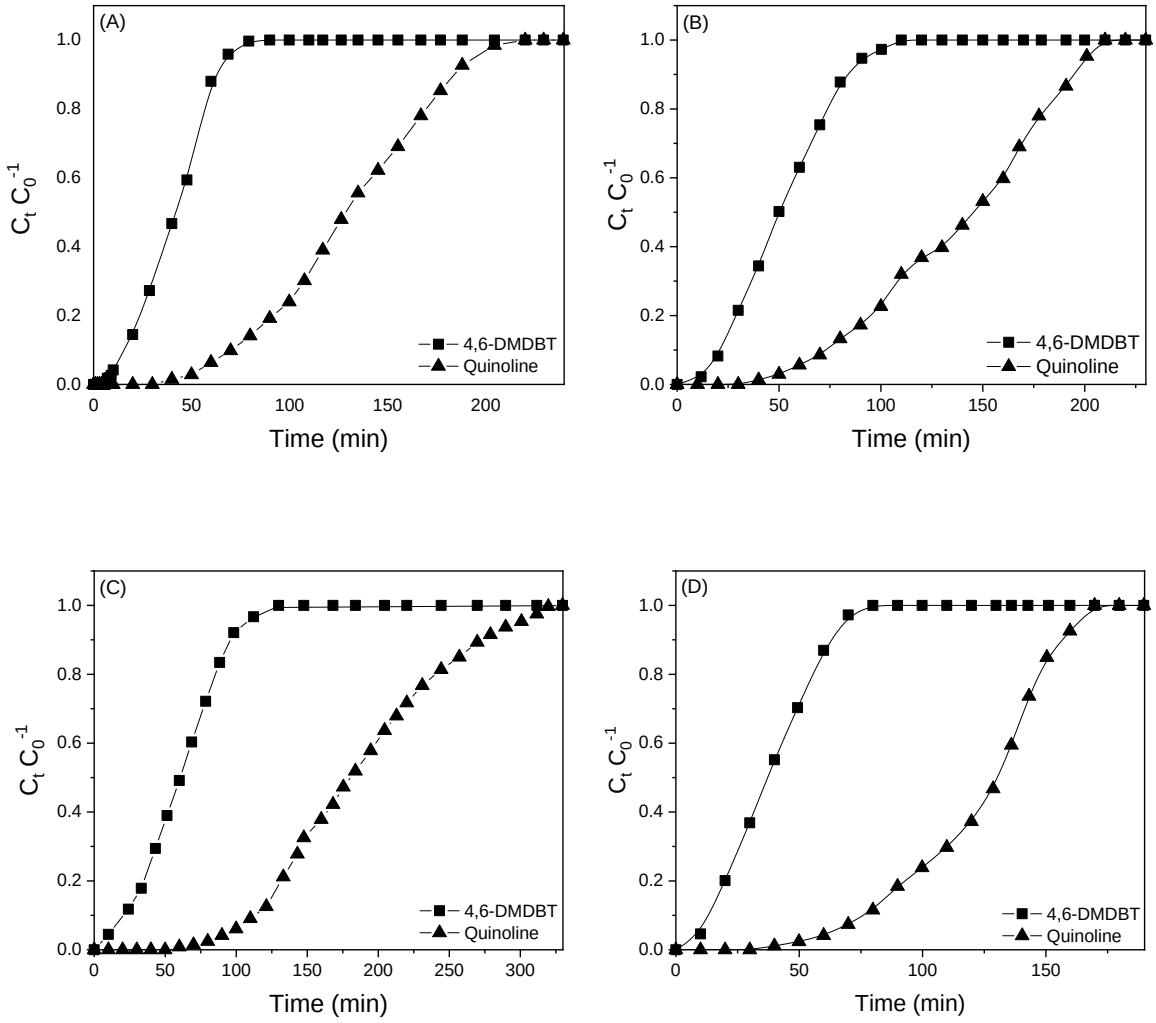

Figure 2. Adsorption curves for 4,6-DMDBT (squares) and QN (dots) for: (**A**) γ-Al_2O_3; (**B**) B(0.4) γ-Al_2O_3; (**C**) Ni(4.0) γ-Al_2O_3 and (**D**) Ni(4.0) B(0.4) γ-Al_2O_3.

The comparison of the adsorption of 4,6-DMDBT and QN on the other supports used in hydrotreating (HT) reactions indicate that the adsorption capacity is dependent on factors such as specific surface area, adsorption pH, density and acid strength, among others [41,42]. For example, we studied the adsorption of 4,6-dimethyldibenzothiophene (4,6-DMDBT) on different supports (SiO_2, Al_2O_3, zeolite 4A, zeolite 13X, natural zeolite, and activated carbon). Despite that the higher adsorption was observed on active carbon due to the high specific surface area, the alumina also exhibits considerable adsorption capacity, which would be related to the presence of OH^- functional groups, which may also have a certain adsorption capacity [43].

On the other hand, the incorporation of boron or nickel to γ-Al_2O_3 increases the q_e values of QN and 4,6-DMDBT. The increases of adsorption values of QN and 4,6-DMDBT by the B(0.4) γ-Al_2O_3 system can be attributed to the increase of the acidity of the adsorbent, produced by the incorporation of boron to alumina [44]. In the case of the Ni (4.0) γ-Al_2O_3 system, the better adsorption of both molecules should be due to the proven ability of Ni to interact with nitrogen or sulfur organic rings through the π-complexation mechanism. In this mechanism, the metallic cation can form the usual σ bonds with their s-orbitals, while their d-orbitals can back-donate electron density to the antibonding π-orbitals of the sulfur or nitrogen rings [7].

When the nickel was incorporated into B(0.4) γ-Al_2O_3, a decrease in the values of q_e of QN and 4,6-DMDBT was observed. These results demonstrated that the boron did not improve the dispersion of nickel on the alumina to the concentrations of metals used, as was evidenced in the other similar

works [45]. The change in the acidity and the IEP values of Ni(4.0) B(0.4) γ-Al_2O_3 adsorbent in comparison with the Ni (4.0) γ-Al_2O_3 could indicates a possible formation of a mixed species of nickel-boron, with lower adsorption capacity of QN and 4,6-DMDBT. In this context, Graff et al. [46], studied the formation of triborate nickel complex in an experiment based on electrochemical reactions and pH monitoring, in which nickel ions were gradually formed by the oxidation of a nickel metal electrode in a solution of boric acid. The authors demonstrated that nickel cations could react with the triborate, forming a complex between both elements. However, the possible formation of a boron nickel complex on the surface of the alumina must be probed with additional characterization techniques.

In terms of selectivity ($\alpha_{i\text{-}n}$), it is possible to observe in all cases that QN is favored in the adsorption with respect to 4,6-DMDBT. However, this selectivity varies depending on the adsorbent used. This behavior have been observed by diverse authors, establishing that the π-complexation adsorbents exhibit high capacity, but low selectivity for sulfur compounds as the result of competitive adsorption of the aromatic compounds [6,47–53]. The selectivity to QN for B(0.4) γ-Al_2O_3 adsorbent decreases with respect to unmodified γ-Al_2O_3, possibly due to a decrease in the Lewis sites of Al(III) when boron is incorporated. Subsequently, the incorporation of nickel generates an increase in the selectivity of QN, probably due to the increase in the acidity of the adsorbents, which can be attributed to the generation of Lewis sites of Ni(II) on the surface of the alumina. Finally, in a mixed system of boron and nickel, the selectivity decreases, due to a combined effect of both elements. Similar results of selectivity were obtained by authors that studied the simultaneous adsorption of sulfur and nitrogen molecules. In this respect, Thaligari et al. studied the simultaneous removal of the dibenzothiophene and quinoline by using zinc impregnated granular activated carbon (Zn-GAC). The study, which used a Taguchi's experimental design methodology, demonstrated a higher adsorption of quinoline in comparison to dibenzothiophene [54]. Likewise, Mohammadian et al. found that the adsorption selectivity of all adsorbents for nitrogen was slightly higher than for sulfur, when studying the desulfurization and denitrogenation of a model fuel containing benzothiophene (BT), dibenzothiophene (DBT), quinoline and carbazole, using MSU-S, CeO_2-MSU-S, and Cu_2O-MSU-S adsorbents [22].

3.2. Adsorption Kinetics

The kinetics parameters obtained by the three models studied for 4,6-DMDBT and QN adsorption, are shown in Tables 3 and 4, respectively. Firstly, the values of the regression coefficient (r^2) obtained for all systems studied are very close to one, which demonstrates that the three models agree with the experimental data.

By using the Yoon–Nelson model, it can be noted that the adsorption capacity is directly related to the values of tau, which corresponds to the time in which 50% of the adsorption has been reached. Therefore, this model can be used to estimate how high the adsorption capacity of the material will be, and how long the saturation of the adsorbent takes.

Table 3. Kinetics parameters obtained by the three models studied for 4,6-DMDBT.

Adsorbent	**Exp**	**Yoon-Nelson** $\frac{C_t}{C_0}=\frac{1}{1+e^{k_{YN}(\tau-t)}}$			**Yan** $\frac{C_t}{C_0}=1-\frac{1}{1+(\frac{C_0\,Q\,t}{q_e m})^a}$			**Thomas** $\frac{C_t}{C_0}=\frac{1}{1+e^{[(k_{th}\,q_e\,m/Q)-(k_{th}\,C_0\,t)]}}$		
	q_e	k_{yn}	tau	r^2	a	q_e	r^2	k_{th}	q_e	r^2
γ-Al_2O_3	7.02	0.10	41.39	0.9981	3.91	6.76	0.9952	0.57	7.13	0.9981
B(0.4) γ-Al_2O_3	8.72	0.07	51.04	0.9977	3.58	8.31	0.9927	0.40	8.80	0.9977
Ni(4.0) γ-Al_2O_3	9.77	0.06	60.07	0.9987	3.51	9.88	0,9904	0.33	10.35	0.9987
Ni(4.0) B(0.4) γ-Al_2O_3	6.51	0.09	37.50	0.9970	3.40	6.07	0.9897	0.51	6.46	0.9970

Table 4. Kinetics parameters obtained by the three models studied for QN.

Adsorbent	Exp	Yoon-Nelson $\frac{C_t}{C_0}=\frac{1}{1+e^{k_{YN}(\tau-t)}}$			Yan $\frac{C_t}{C_0}=1-\frac{1}{1+(\frac{C_0\,Q\,t}{q_e m})^a}$			Thomas $\frac{C_t}{C_0}=\frac{1}{1+e^{[(k_{th}\,q_e\,m/Q)-(k_{th}\,C_0\,t)]}}$		
	q_e	k_{yn}	tau	r^2	a	q_e	r^2	k_{th}	q_e	r^2
γ-Al_2O_3	22.29	0.04	129.89	0.9948	4.96	21.82	0.9938	0.22	22.37	0.9981
B(0.4) γ-Al_2O_3	23.69	0.03	140.28	0.9888	4.75	23.49	0.9759	0.20	24.19	0.9888
Ni(4.0) γ-Al_2O_3	32.67	0.03	183.08	0.9962	4.84	30.72	0.9971	0.16	31.55	0.9962
Ni(4.0) B(0.4) γ-Al_2O_3	21.02	0.05	125.46	0.9882	7.24	21.40	0.9778	0.33	21.61	0.9881

In the case of the Yan model, although this model as mentioned above is used in pharmacological studies, when applied in the adsorption of the different molecules under study, the r^2 values fits well with the experimental data, so this model could be used to also predict the adsorption curves of these compounds.

As can see in Table 3, both the Thomas and Yan models can predict the results of adsorption capacity (q_e). However, if we calculate the residual sum of squares (RSS) between the experimental and predicted values for each model, the Thomas model has closer values to zero than the Yan model. For instance, in the case of 4,6-DMDBT the RSS value for the Thomas model is 0.35, which is lower than the value obtained for the Yan Model (0.44). For QN the differences between the RSS for the two models are higher: in the case of the Thomas model, the RSS value is 1.86 and for the Yan model is 4.20. This indicates that the Thomas model predicts better the q_e values.

Moreover, the Thomas model delivers more information about the adsorption process. Taking into account the considerations of the model, it is possible to establish that the adsorption process of the molecules follows a reversible kinetic of second order, where all adsorption sites are equivalent and each of these sites can contain a molecule adsorbed which does not interact with adjacent sites. Likewise, the information obtained allows the determination of the kinetic constant of the adsorption process of 4,6-DMDBT and QN on the studied adsorbents. On this matter, it is possible to establish that the kinetic constant obtained by this model is inversely proportional to the adsorption capacity of the different materials studied, due probably to the longer contact time used in the interaction between the molecule and the adsorbent. This is seen more clearly in Figure 3.

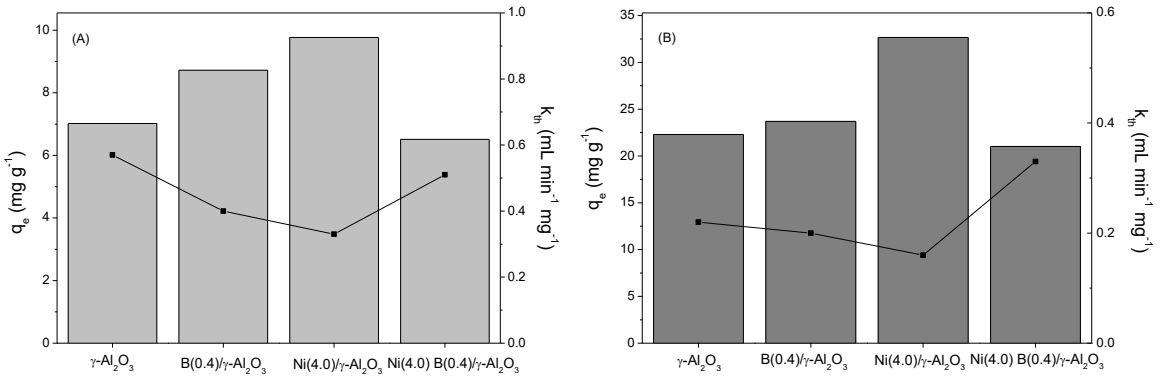

Figure 3. Adsorption capacities (bars) and Thomas kinetic constants (dots) obtained for the different adsorbents: (**A**) 4.6-DMDBT and (**B**) QN.

4. Conclusions

Among the adsorbents studied in this work, Ni(4.0) γ-Al_2O_3 has the better performance for the simultaneous adsorption of quinoline and 4,6-DMDBT, this due to its higher acidity and capacity to generate π-complexation between the molecule and the adsorbent. The Ni(4.0) B(0.4) γ-Al_2O_3 adsorbent has a lower adsorption capacity of both molecules, presumably due to formation of a mixed species of nickel-boron. In terms of selectivity, QN is favored in the adsorption with respect to

4,6-DMDBT, due to its basic nature. In all adsorbent systems studied, the adsorption curves fitted well with the three models, which show high r^2 values. However, the Thomas model predicts better the adsorption capacity values, and also gives more information about the adsorption process.

Author Contributions: Writing—original draft, E.C.; Writing—review & editing, E.C., J.O., G.A., and P.B.; Investigation, E.C., B.P., C.M., F.R.; Conceptualization, E.C., J.O., P.B, Formal Analysis, E.C., J.O., G.A., P.B.; Funding acquisition, E.C. and P.B.; Supervision, P.B. All authors have read and agreed to the published version of the manuscript.

Funding: This work was financed by the CONICYT PFCHA/DOCTORADO NACIONAL/2013—21130871 and DI Consolidado PUCV N°039369.

Conflicts of Interest: The authors declare no conflict of interest.

References

1. Muzic, M.; Sertic-Bionda, K.; Gomzi, Z.; Podolski, S.; Telen, S. Study of diesel fuel desulfurization by adsorption. *Chem. Eng. Res. Des.* **2010**, *88*, 487–495. [CrossRef]
2. Furimsky, E.; Massoth, F.E. Deactivation of hydroprocessing catalysts. *Catal. Today* **1999**, *52*, 381–495. [CrossRef]
3. Peralta, C.; Camú, E.; Bassi, R.; Villarroel, M.; Ojeda, J.; Baeza, P. Denitrogenation by Adsorption of Pyridine on Ni / Support Adsorbents. *J. Chil. Chem. Soc.* **2016**, *4*, 3211–3213. [CrossRef]
4. Kim, J.H.; Ma, X.; Zhou, A.; Song, C. Ultra-deep desulfurization and denitrogenation of diesel fuel by selective adsorption over three different adsorbents: A study on adsorptive selectivity and mechanism. *Catal. Today* **2006**, *111*, 74–83. [CrossRef]
5. Xue, L.; Zhang, D.; Xu, Y.; Liu, X. Adsorption of thiophene compounds on MoO_3/γ-Al_2O_3 catalysts with different mesopore sizes. *Microporous Mesoporous Mater.* **2017**, *238*, 46–55. [CrossRef]
6. Sarda, K.K.; Bhandari, A.; Pant, K.K.; Jain, S. Deep desulfurization of diesel fuel by selective adsorption over Ni/Al_2O_3 and Ni/ZSM-5 extrudates. *Fuel* **2012**, *93*, 86–91. [CrossRef]
7. Hernández-Maldonado, A.J.; Yang, R.T. Desulfurization of diesel fuels via π-Complexation with Nickel(II)-exchanged X- and Y-Zeolites. *Ind. Eng. Chem. Res.* **2004**, *43*, 1081–1089. [CrossRef]
8. Singh, S.B.; De, M. Room Temperature Adsorptive Removal of Thiophene over Zinc Oxide-Based Adsorbents. *J. Mater. Eng. Perform.* **2018**, *27*, 2661–2667. [CrossRef]
9. Zhang, Y.; Liu, D.; Zhou, L.; Tang, M.; Li, X.; Yang, Y. A mullite etching route to tabular α-alumina crystals and application in adsorption desulfurization for dibenzothiophene. *Fuel* **2018**, *216*, 10–15. [CrossRef]
10. Baia, L.V.; Souza, W.C.; De Souza, R.J.F.; Veloso, C.O.; Chiaro, S.S.X.; Figueiredo, M.A.G. Removal of Sulfur and Nitrogen Compounds from Diesel Oil by Adsorption Using Clays as Adsorbents. *Energy Fuels* **2017**, *31*, 11731–11742. [CrossRef]
11. Liu, Y.; Pan, Y.; Wang, H.; Liu, Y.; Liu, C. Ordered mesoporous $Cu\text{-}ZnO\text{-}Al_2O_3$ adsorbents for reactive adsorption desulfurization with enhanced sulfur saturation capacity. *Chin. J. Catal.* **2018**, *39*, 1543–1551. [CrossRef]
12. Zhang, D.; Xue, L.; Xu, Y.; Song, L.; Liu, X. Adsorption of 4,6-dimethyldibenzothiophene and collidine over MoO_3/γ-Al_2O_3 catalysts with different pore structures. *J. Colloid Interface Sci.* **2017**, *493*, 218–227. [CrossRef] [PubMed]
13. Latifi, S.M.; Azghandi, J.B.; Salehirad, A.; Parvini, M. A comparative study on H_2S removal using Mg–Al spinel ($MgAl_2O_4$) and MgO/Al_2O_3 nanocomposites. *Chin. J. Chem. Eng.* **2017**, *25*, 1329–1334. [CrossRef]
14. Sun, M.; Nicosia, D.; Prins, R. The effects of fluorine, phosphate and chelating agents on hydrotreating catalysts and catalysis. *Catal. Today* **2003**, *86*, 173–189. [CrossRef]
15. Villarroel, M.; Baeza, P.; Gracia, F.; Escalona, N.; Avila, P.; Gil-Llambías, F.J. Phosphorus effect on Co//Mo and Ni//Mo synergism in hydrodesulphurization catalysts. *Appl. Catal. A Gen.* **2009**, *364*, 75–79. [CrossRef]
16. Méndez, A.; Villarroel, M.; Camú, E.; Ávila, P.; Baeza, P. Effect of Fluorine in the Synergism Co-Mo Via Hydrogen Spillover on the HydrodesulPhurization Of Refractory Molecules. *J. Chil. Chem. Soc.* **2013**, *4*, 2067–2070. [CrossRef]
17. Rashidi, F.; Sasaki, T.; Rashidi, A.M.; Nemati Kharat, A.; Jozani, K.J. Ultradeep hydrodesulfurization of diesel fuels using highly efficient nanoalumina-supported catalysts: Impact of support, phosphorus, and/or boron on the structure and catalytic activity. *J. Catal.* **2013**, *299*, 321–335. [CrossRef]

18. Escobar, J.; Barrera, M.C.; Gutiérrez, A.W.; Terrazas, J.E. Benzothiophene hydrodesulfurization over NiMo/alumina catalysts modified by citric acid. Effect of addition stage of organic modifier. *Fuel Process. Technol.* **2017**, *156*, 33–42. [CrossRef]
19. Escobar, J.; Barrera, M.C.; Gutiérrez, A.W.; Cortés-Jacome, M.A.; Angeles-Chávez, C.; Toledo, J.A.; Solís-Casados, D.A. Highly active P-doped sulfided NiMo/alumina HDS catalysts from Mo-blue by using saccharose as reducing agents precursor. *Appl. Catal. B Environ.* **2018**, *237*, 708–720. [CrossRef]
20. van Haandel, L.; Bremmer, G.M.; Hensen, E.J.M.; Weber, T. The effect of organic additives and phosphoric acid on sulfidation and activity of (Co)Mo/Al_2O_3 hydrodesulfurization catalysts. *J. Catal.* **2017**, *351*, 95–106. [CrossRef]
21. Han, W.; Nie, H.; Long, X.; Li, M.; Yang, Q.; Li, D. Effects of the support BrØnsted acidity on the hydrodesulfurization and hydrodenitrogention activity of sulfided NiMo/Al_2O_3 catalysts. *Catal. Today* **2017**, *292*, 58–66. [CrossRef]
22. Mohammadian, M.; Khosravi-Nikou, M.R.; Shariati, A.; Aghajani, M. Model fuel desulfurization and denitrogenation using copper and cerium modified mesoporous material (MSU-S) through adsorption process. *Clean Technol. Environ. Policy* **2018**, *20*, 95–112. [CrossRef]
23. Ma, X.; Sprague, M.; Song, C. Deep desulfurization of gasoline by selective adsorption over nickel-based adsorbent for fuel cell applications. *Ind. Eng. Chem. Res.* **2005**, *44*, 5768–5775. [CrossRef]
24. Hernandez-Maldonado, A.J.; Stamatis, S.D.; Yang, R.T.; He, A.Z.; Cannella, W. New sorbents for desulfurization of diesel fuels via pi complexation: Layered beds and regeneration. *Ind. Eng. Chem. Res.* **2004**, *43*, 769–776. [CrossRef]
25. Zheng, S.; Liu, B.S.; Wang, W.S.; Wang, F. Mesoporous and Macroporous Alumina-Supported Nickel Adsorbents for Adsorptive Desulphurization of Commercial Diesel. *Adsorpt. Sci. Technol.* **2015**, *33*, 337–353. [CrossRef]
26. Chen, W.; Maugé, F.; van Gestel, J.; Nie, H.; Li, D.; Long, X. Effect of modification of the alumina acidity on the properties of supported Mo and CoMo sulfide catalysts. *J. Catal.* **2013**, *304*, 47–62. [CrossRef]
27. Ding, L.; Zhang, Z.; Zheng, Y.; Ring, Z.; Chen, J. Effect of fluorine and boron modification on the HDS, HDN and HDA activity of hydrotreating catalysts. *Appl. Catal. A Gen.* **2006**, *301*, 241–250. [CrossRef]
28. Ferdous, D.; Dalai, A.K.; Adjaye, J. A series of NiMo/Al_2O_3 catalysts containing boron and phosphorus. *Appl. Catal. A Gen.* **2004**, *260*, 137–151. [CrossRef]
29. Usman, U.; Takaki, M.; Kubota, T.; Okamoto, Y. Effect of boron addition on a MoO_3/Al_2O_3 catalyst. *Appl. Catal. A Gen.* **2005**, *286*, 148–154. [CrossRef]
30. Curtin, T.; McMonagle, J.B.; Hodnett, B.K. Influence of boria loading on the acidity of B_2O_3/Al_2O_3 catalysts for the conversion of cyclohexanone oxime to caprolactam. *Appl. Catal. A Gen.* **1992**, *93*, 91–101. [CrossRef]
31. Yoon, Y.H.E.E.; Nelson, J.H. Application of Gas Adsorption Kinetics—II. A Theoretical Model for Respirator Cartridge Service Life and Its Practical Applications. *Am. Ind. Hyg. Assoc. J.* **1984**, *45*, 517–524. [CrossRef] [PubMed]
32. Yan, G.; Viraraghavan, T.; Chen, M. A New Model for Heavy Metal Removal in a Biosorption Column. *Adsorpt. Sci. Technol.* **2001**, *19*, 25–43. [CrossRef]
33. Thomas, H.C. Chromatography: A problem in kinetics. *Ann. N. Y. Acad. Sci.* **1946**, *36*, 161–182. [CrossRef] [PubMed]
34. Brunauer, S.; Emmett, P.H.; Teller, E. Adsorption of Gases in Multimolecular Layers. *J. Am. Chem. Soc.* **1938**, *60*, 309–319. [CrossRef]
35. Cid, R.; Pecchi, G. Potentiometric Method for Determining the Number and Relative Strength of Acid Sites in Colored Catalysts. *Appl. Catal.* **1985**, *14*, 15–21. [CrossRef]
36. Xu, Z.; Cai, J.; Pan, B. Mathematically modeling fixed-bed adsorption in aqueous systems. *J. Zhejiang Univ. Sci. A* **2013**, *14*, 155–176. [CrossRef]
37. Engels, S.; Herold, E.; Lausch, H.; Mayr, H.; Meiners, H.W.; Wilde, M. Boron-An Acidity and Texture Modifier for Alumina Supported Catalysts. In *Studies in Surface Science and Catalysis*; Elsevier: Cambridge, MA, USA, 1993.
38. Cordero, R.L.; Gil Llambías, F.J.; Palacios, J.M.; Fierro, J.L.G.; Agudo, A.L. Surface changes of alumina induced by phosphoric acid impregnation. *Appl. Catal.* **1989**, *56*, 197–206. [CrossRef]

39. Barale, M.; Lefèvre, G.; Carrette, F.; Catalette, H.; Fédoroff, M.; Cote, G. Effect of the adsorption of lithium and borate species on the zeta potential of particles of cobalt ferrite, nickel ferrite, and magnetite. *J. Colloid Interface Sci.* **2008**, *328*, 34–40. [CrossRef]
40. Laredo, G.C.; Vega-Merino, P.M.; Pérez-Romo, P.; Navarrete-Bolaños, J.; Trejo-Zárraga, F. Adsorption of nitrogen compounds from diesel fuels over alumina-based adsorbent towards ULSD production. *Pet. Sci. Technol.* **2017**, *35*, 392–398. [CrossRef]
41. Xu, H.; Sun, X.; Yu, Y.; Liu, G.; Ma, L.; Huang, G. Removal of quinoline using various particle sizes anthracite: Adsorption kinetics and adsorption isotherms. *Physicochem. Probl. Miner. Process.* **2019**, *55*, 196–207.
42. Helmy, A.K.; De Bussetti, S.G.; Ferreiro, E.A. Adsorption of quinoline from aqueous solutions by some clays and oxides. *Clays Clay Miner.* **1983**, *31*, 29–36. [CrossRef]
43. Aparicio, F.; Camú, E.; Villarroel, M.; Escalona, N.; Baeza, P. Deep desulfurization by adsorption of 4,6-dimethyldibenzothiophene, study of adsorption on different transition metal oxides and supports. *J. Chil. Chem. Soc.* **2013**, *58*, 2057–2060. [CrossRef]
44. Flego, C. Characterization of γ-alumina and borated alumina catalysts. *Appl. Catal. A Gen.* **1999**, *185*, 137–152. [CrossRef]
45. Li, D.; Sato, T.; Imamura, M.; Shimada, H.; Nishijima, A. Spectroscopic Characterization of Ni-Mo/γ-Al_2O_3-B_2O_3 Catalysts for Hydrodesulfurization of Dibenzothiophene. *J. Catal.* **1997**, *170*, 357–365. [CrossRef]
46. Graff, A.; Barrez, E.; Baranek, P.; Bachet, M.; Bénézeth, P. Complexation of Nickel Ions by Boric Acid or (Poly)borates. *J. Solution Chem.* **2017**, *46*, 25–43. [CrossRef]
47. Velu, S.; Ma, X.; Song, C. Selective Adsorption for Removing Sulfur from Jet Fuel over Zeolite-Based Adsorbents. *Ind. Eng. Chem. Res.* **2003**, *42*, 5293–5304. [CrossRef]
48. Xue, M.; Chitrakar, R.; Sakane, K.; Hirotsu, T.; Ooi, K.; Yoshimura, Y.; Feng, Q.; Sumida, N. Selective adsorption of thiophene and 1-benzothiophene on metal-ion-exchanged zeolites in organic medium. *J. Colloid Interface Sci.* **2005**, *285*, 487–492. [CrossRef]
49. Bhattacharjee, S.; Chen, C.; Ahn, W.S. Chromium terephthalate metal-organic framework MIL-101: Synthesis, functionalization, and applications for adsorption and catalysis. *RSC Adv.* **2014**, *4*, 52500–52525. [CrossRef]
50. Chen, H.; Wang, Y.; Yang, F.H.; Yang, R.T. Desulfurization of high-sulfur jet fuel by mesoporous π-complexation adsorbents. *Chem. Eng. Sci.* **2009**, *64*, 5240–5246. [CrossRef]
51. Meng, C.; Fang, Y.; Jin, L.; Hu, H. Deep desulfurization of model gasoline by selective adsorption on Ag+/Al-MSU-S. *Catal. Today* **2010**, *149*, 138–142. [CrossRef]
52. Yang, L.; Wang, S.; Wang, R.; Yu, H. Selective Removal of Nitrogen-Containing Heterocyclic Compounds from Transportation Diesel Fuels with Reactive Adsorbent. *Chin. J. Chem. Eng.* **2013**, *21*, 558–563. [CrossRef]
53. Song, H.; Chang, Y.; Wan, X.; Dai, M.; Song, H.; Jin, Z. Equilibrium, Kinetic, and Thermodynamic Studies on Adsorptive Desulfurization onto CuICeIVY Zeolite. *Ind. Eng. Chem. Res.* **2014**, *53*, 5701–5708. [CrossRef]
54. Thaligari, S.K.; Srivastava, V.C.; Prasad, B. Simultaneous Adsorptive Desulfurization and Denitrogenation by Zinc Loaded Activated Carbon: Optimization of Parameters. *Pet. Sci. Technol.* **2015**, *33*, 1667–1675. [CrossRef]